IOPscience iopscience.iop.org

Home Search Collections Journals About Contact us My IOPscience

Raman and infrared vibrational frequencies and elastic properties of solid BaFCl calculated with various Hamiltonians: an *ab initio* study

This article has been downloaded from IOPscience. Please scroll down to see the full text article.

2005 J. Phys.: Condens. Matter 17 535

(http://iopscience.iop.org/0953-8984/17/3/012)

View the table of contents for this issue, or go to the journal homepage for more

Download details:
IP Address: 129.252.86.83
The article was downloaded on 27/05/2010 at 19:46

Please note that terms and conditions apply.

INSTITUTE OF PHYSICS PUBLISHING JOURNAL OF PHYSICS: CONDENSED MATTER

J. Phys.: Condens. Matter **17** (2005) 535–548 doi:10.1088/0953-8984/17/3/012

Raman and infrared vibrational frequencies and elastic properties of solid BaFCl calculated with various Hamiltonians: an *ab initio* study

Mohammadou Mérawa[1,4], **Yves Noël**[2], **Bartolomeo Civalleri**[3], **Ross Brown**[1] **and Roberto Dovesi**[3]

[1] Laboratoire de Chimie Théorique et de Physico-Chimie Moléculaire, UMR 5624, FR 'IPREM' 2606, BP 27540 IFR—rue Jules Ferry 64075 Pau-Cedex, France
[2] Laboratoire de Pétrologie et Modélisation des Materiaux et des Processus, Université P & M Curie Paris 6, 4 place Jussieu 75252 Paris Cedex 05, France
[3] Dipartimento di Chimica IFM, University of Torino, Via Giuria 7, I-10125 Torino, Italy

E-mail: mohammadou.merawa@univ-pau.fr

Received 12 August 2004, in final form 7 December 2004
Published 7 January 2005
Online at stacks.iop.org/JPhysCM/17/535

Abstract

The structural, elastic, vibrational and electronic properties of barium fluorochloride (BaFCl) have been investigated for the first time at the *ab initio* level, by using the periodic CRYSTAL program. Both Hartree–Fock (HF) and density functional theory (DFT) Hamiltonians have been used, with the latter in its local density (LV), gradient-corrected (PP), and hybrid (B3LYP) versions. All properties, and in particular the phonon frequencies and the elastic constants, are strongly Hamiltonian dependent. The structural features are in reasonable agreement with experiment, the percentage deviation being smaller than 5% in all cases. The B3LYP elastic constants are in good agreement with experiment, whereas LV systematically overestimates them. PP and B3LYP provide the best results for the vibrational frequencies, the mean percentage absolute difference with respect to experiment being 2.9 and 4.3%, for Raman and 4.8 and 6.3%, for infrared mode frequencies, respectively.

(Some figures in this article are in colour only in the electronic version)

1. Introduction

In recent years, the elastic properties and phonon spectra of the alkaline-earth fluorohalides MFX (M = Ba, Ca, Sr; X = Cl, Br, I) have been the subject of many theoretical and experimental

[4] Author to whom any correspondence should be addressed.

 © 2005 IOP Publishing Ltd Printed in the UK

investigations [1–20]. These compounds, when doped with rare-earth ions, present fascinating properties, like those related to image plate x-ray storage [21–24]; they are also used as pressure calibrants [21] in diamond anvil cells. Alkaline-earth fluorohalides are layered ionic compounds belonging to the family of the natural mineral PbFCl, crystallizing in the tetragonal $P4/nmm$ space group [25] (matlockite-type structure).

Recently, Mittal *et al* [26] investigated the lattice dynamics of some MFX compounds by using an interatomic potential. The elastic constants have also been predicted [16, 17] by using a shell-model scheme, and compared with the experimental data obtained from Brillouin scattering (BS) and ultrasonic (US) measurements [6, 19]. We are not aware of any *ab initio* calculation concerning these compounds.

In this paper, we report results concerning the structural, elastic, vibrational and electronic properties of BaFCl, one of the members of the matlockite family. The periodic *ab initio* CRYSTAL program [27], based on a local (Gaussian) basis set, has been used. Four different Hamiltonians have been adopted, namely Hartree–Fock, and DFT in its local [28] (LV) and gradient corrected [29–32] variants (PP), as well as the hybrid B3LYP [33, 34] scheme. This permits a comparison of the performance of the most popular computational schemes in predicting the properties of this material.

Section 2 provides information on the methodological tools and a description of the computational aspects. The numerical results, which include structural parameters, electronic structures, energetic features, elastic constants and phonons vibrational frequencies, are discussed and compared with experimental data in section 3. Unless stated, atomic units are used throughout this paper.

2. Method and computational details

Calculations have been performed with a development version of the periodic *ab initio* CRYSTAL03 program [27]. Crystalline orbitals are represented as linear combinations of Bloch functions (BFs), and are evaluated over a regular three-dimensional mesh in reciprocal space. Each BF is built from local atomic orbitals (AOs), which are contractions (linear combinations with constant coefficients) of Gaussian-type functions (GTFs), each GTF being the product of a Gaussian times a real solid spherical harmonic. All electron basis sets have been used for Cl and F atoms [35, 36]. They consist of 8-6311(1) and 7-311(1) contractions for Cl and F, respectively, where the first figure refers to an s shell, the others to sp shells; d shell contractions are given in parentheses. There are then 22 and 18 AOs for Cl and F, respectively. The exponents of the outer sp and d shells have been re-optimized at the HF level (and used as such for the other Hamiltonians) to the following values (in bohr^{-2} units): $\alpha(\mathrm{Cl, sp}) = \{0.424, 0.150\}$, $\alpha(\mathrm{Cl, d}) = 0.250$; $\alpha(\mathrm{F, sp}) = \{0.443, 0.166\}$, $\alpha(\mathrm{F, d}) = 0.280$. A Hay–Wadt [37–39] effective core potential (ECP) has been adopted for barium; 31(1) contractions of GTFs have been used for the valence electrons (the optimized exponents are: $\alpha(\mathrm{Ba, sp}) = 0.219$; $\alpha(\mathrm{Ba, d}) = 0.303$). The influence of the basis set effects in the calculation of the properties investigated in this work has already been discussed in [36]. Standard values for the computational tolerances as defined in the CRYSTAL03 manual [27] have been adopted for all steps of the calculation, except for the vibrational frequencies, that require more severe conditions.

In the geometry optimization, a structural relaxation procedure consisting of two independent steps was iteratively performed. In the first step, the cell parameters (a, b, c) were optimized with the atoms at fixed positions. Cell optimization was carried out by means of a modified Polak–Ribière algorithm, in which the energy gradients were evaluated numerically by means of the central-difference formula [40]. In the second step, the atomic

positions (x, y, z, fractional coordinates) were fully relaxed at fixed cell parameters. The forces on the atoms were obtained by using the analytical HF [41, 42] and DFT [43] energy gradients and were used to relax the atoms to equilibrium by using a modified conjugate gradient algorithm proposed by Schlegel [44]. Convergence was tested on the RMS and the absolute value of the largest component of the gradients and the estimated displacements. The threshold for the maximum force, the RMS force, the maximum atomic displacement, and the RMS atomic displacement on all atoms have been set to 0.000 45, 0.000 30, 0.001 80 and 0.001 20 au, respectively. The atomic position optimization was considered complete when these four conditions were satisfied. The crystal symmetry was maintained during the optimization process. The two-step structure optimization process was repeated until both the cell parameters and the atomic positions convergence criteria were satisfied [45].

As regards the Hamiltonian, in the large variety of local and non-local exchange–correlation potentials available, three functional forms have been chosen. They are indicated as follows.

- LV for local [28] exchange plus Vosko–Wilk–Nusair [46] correlation potential.
- PP for Perdew–Wang [29–32] exchange and correlation potential.
- B3LYP [33, 34] for Becke's three-parameter exchange–correlation functional which includes local and gradient corrected exchange and correlation functionals and in addition Hartree–Fock exchange.
- HF for Hartree–Fock completes the set.

The results have thus been obtained with four different Hamiltonians, giving some insight into the differences one can expect when changing this important parameter of the calculation.

A Taylor expansion of the unit cell energy to second order as a function of the strain,

$$E(\varepsilon) = E(0) + \sum_{i=1}^{6}\left[\frac{\partial E}{\partial \varepsilon_i}\right]_0 \varepsilon_i + \frac{1}{2}\sum_{i,j=1}^{6}\left[\frac{\partial^2 E}{\partial \varepsilon_i \varepsilon_j}\right]_0 \varepsilon_i \varepsilon_j,$$

has been considered for the calculation of the elastic constants. $E(0)$ stands for the energy of the equilibrium configuration, and ε_i refers to the strain components expressed according to Voigt's notation with a single index ($i = 1, 6$). The elastic constants, C_{ij}, are related to the second derivatives of the energy with respect to strain components as follows:

$$C_{ij} = \frac{1}{V}\left[\frac{\partial^2 E}{\partial \varepsilon_i \partial \varepsilon_j}\right]_0.$$

Energy second derivatives are evaluated numerically. Since BaFCl is a tetragonal crystal with a D_{4h}^7 space group, there are six non-vanishing independent components of the elastic tensor, namely C_{11}, C_{12}, C_{13}, C_{33}, C_{44} and C_{66}. Fifteen ε_i values in the interval $[-0.020, +0.020]$ Å interval have been considered for the fitting. During the deformation of the unit cell with a given strain, the symmetry may be reduced and additional degrees of freedom appear that must be fully relaxed.

For this tetragonal system, the linear compressibilities parallel ($\parallel$) and perpendicular ($\perp$) to the C_4 axis are related to the elastic constants in the following way:

$$\chi_\parallel = \frac{C_{11} + C_{12} - 2C_{13}}{[C_{33}(C_{11} + C_{12}) - 2C_{13}^2]}$$
$$\chi_\perp = \frac{C_{33} - C_{13}}{[C_{33}(C_{11} + C_{12}) - 2C_{13}^2]}.$$

The volume compressibility χ, given by $\chi = \chi_\parallel + 2\chi_\perp$, can then be evaluated.

We refer to a recent paper [47] for a complete discussion of the computational conditions and other numerical aspects concerning the calculation of the phonon frequencies at the $\Gamma = (0, 0, 0)$ point. The mass-weighted Hessian matrix is obtained by numerical differentiation of the analytical first derivatives, calculated at geometries obtained by incrementing in turn each of the $3N$ nuclear coordinates by a small amount u with respect to the equilibrium geometry. In the case of ionic compounds, long-range Coulomb effects due to coherent displacement of the crystal nuclei are neglected in the above calculation, as a consequence of imposing the periodic boundary conditions [48]. The mass-weighted Hessian needs to be corrected in order to obtain the longitudinal optical (LO) modes [49]. The electronic dielectric and Born charge tensors have therefore been calculated with the four Hamiltonians. The components of the Born charge tensor, e^*, are defined (see for example [50]) as the partial derivative of the macroscopic polarization, P, with respect to a periodic displacement, u, of the ath atom at zero macroscopic electric field, E:

$$e^{*\,a}_{ij} = V\left[\frac{\partial P_i}{\partial u^a_j}\right]_{E=0},$$

where $i, j = x, y, z$ and V is the volume of the unit cell.

As regards the grid for the numerical integration of the exchange–correlation term, 75 radial points (the default value is 55) and 974 (default 434) angular points in a Lebedev scheme have been used. The condition for the SCF convergence is set to 10^{-10} Hartree. The shrinking factor of the reciprocal space net is set to 8, corresponding to 75 reciprocal space points at which the Hamiltonian matrix was diagonalized. The total energies obtained with this mesh is fully converged.

3. Results and discussion

BaFCl crystallizes in a tetragonal structure as illustrated in figure 1(a). The unit cell has two molecular units. All atoms are in special positions. This compound, like all the fluorohalides of the matlockite family, is characterized by a packing of layers along the c axis. The stacking of these layers is of the type F–Ba–Cl–Cl–Ba–F. The barium is nine-fold coordinated by four F atoms at 2.708 Å (B3LYP optimized geometry), and five Cl atoms, one at 3.288 Å, and four at 3.366 Å (figure 2(a)). The Cl atoms are connected to five Ba atoms in a square pyramidal configuration (figure 2(b)), whereas the F atoms are surrounded by four Ba atoms (figure 2(c)). Each layer has at the centre the F atoms, surrounded above and below by barium planes, followed by planes of Cl atoms. A cleavage plane is therefore formed between the two adjacent Cl planes (see figure 1(b)), separated by 3.853 Å.

The lattice parameters and the interatomic distances calculated with the four Hamiltonians are given in table 1, together with the experimental data [51]. The calculated a and c cell parameters are in excellent agreement with experiment in all cases, but LV provides slightly underestimated values. A quite good agreement with the experiment was obtained at LDA level by Kalpana *et al* [13] ($a = 4.391$ Å; $c = 7.227$ Å) by using a tight-binding linear muffin-tin orbital (TB-LMTO) method. The B3LYP and PP calculated interatomic distances are within 1–3% of the measured values.

The energy data relevant to the calculation of the BaFCl formation energies (ΔE_f), as well as the interlayer energy IE, calculated as the difference between the bulk energy and the energy of an isolated two-dimensional layer, whose fractional coordinates have been re-optimized, are listed in table 2. We have not been able to find any data concerning the experimental formation energy of this compound. We have shown recently [52–54] that the formation energies calculated with B3LYP and PP Hamiltonians are generally quite close to

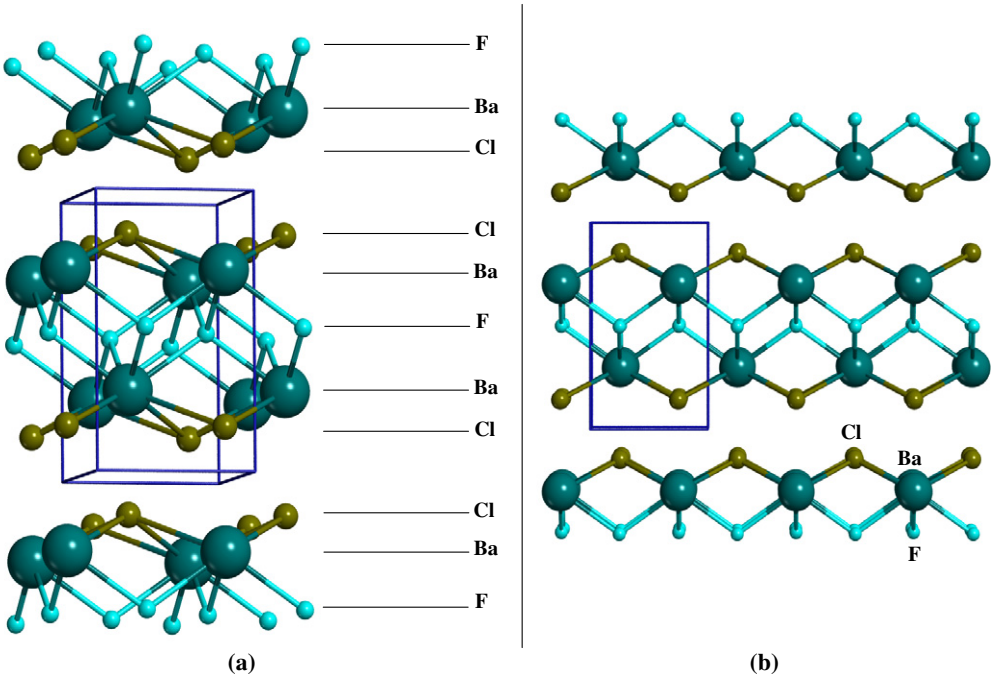

Figure 1. B3LYP optimized structures of BaFCl (a) and of the isolated two-dimensional layer (b).

Table 1. Calculated and experimental equilibrium lattice parameters and interatomic distances (in Å). Percentage deviation with respect to experiment enclosed in parentheses.

	HF	B3LYP	PP	LV	Exp. [51]
a	4.567 (+3.8)	4.494 (+2.2)	4.465 (+1.6)	4.336 (−1.3)	4.394
c	7.478 (+3.4)	7.416 (+2.6)	7.286 (+0.8)	7.062 (−2.3)	7.225
z_{Ba}	0.2003	0.2035	0.2068	0.2082	0.2049
z_{Cl}	0.6495	0.6469	0.6488	0.6522	0.6472
Ba–F	2.731 (+3.0)	2.708 (+2.2)	2.693 (+1.6)	2.620 (−1.1)	2.649
Ba–Cl	3.360 (+4.9)	3.288 (+2.8)	3.221 (+0.8)	3.135 (−1.9)	3.196
F–F	3.229 (+3.8)	3.178 (+2.2)	3.157 (+1.6)	3.066 (−1.3)	3.106
F–Cl	3.476 (+3.2)	3.450 (+2.5)	3.396 (+0.9)	3.276 (−2.6)	3.365
Cl–Cl	3.928 (+4.1)	3.853 (+2.3)	3.830 (+1.7)	3.744 (−0.6)	3.765

the experimental values, and can therefore be considered as good estimates for this quantity. As regards the interlayer energy, the small values (the Basis-Set-Superposition Error (BSSE) has been taken into account) given in the table indicate that the interlayer interaction (IE) is weak, although not so weak as in other cases like in brucite [55], that has been calculated to be only 10% of the present values. BaFCl can thus be seen as a two-dimensional system, with relatively weak interlayer interactions.

The Mulliken net atomic charges (q) and bond populations (b) are collected in table 3. They indicate, as expected, that the Ba–F and Ba–Cl bonds are essentially ionic, since the Ba Mulliken charges are close to +2, and those of F and Cl are close to $-1|e|$. These data remain essentially unaltered when slightly smaller or larger basis sets are used, in spite of the arbitrary nature [56] of the partition of the charge implicit in the Mulliken scheme.

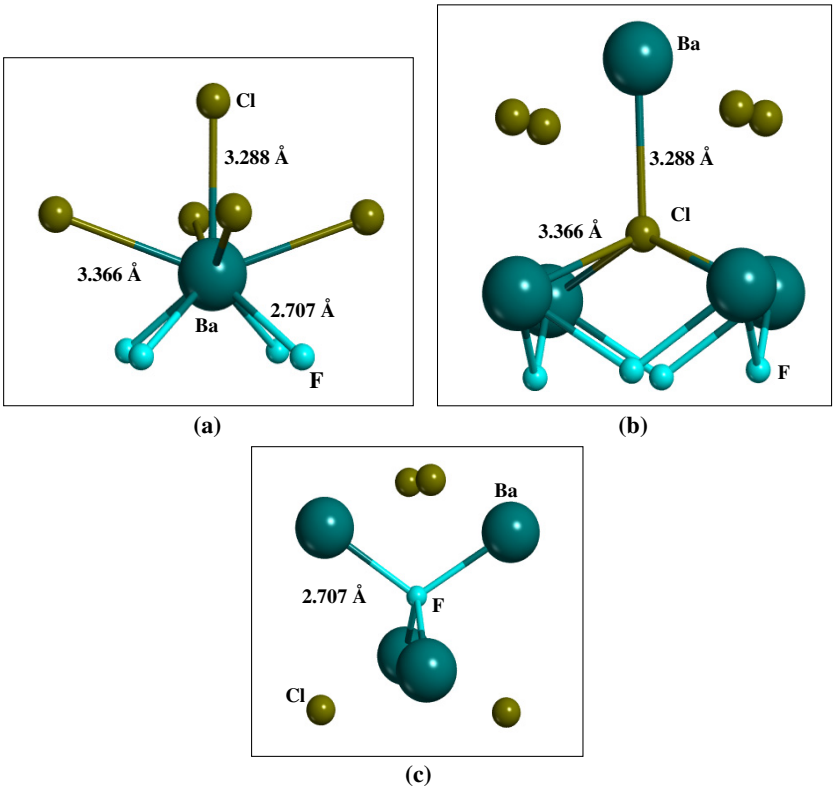

Figure 2. The atomic coordination in BaFCl: (a) Ba; (b) Cl; and (c) F.

Table 2. Total energy of the atoms and BaFCl (per formula unit, in Hartrees). ΔE_f (eV) is the formation energy from the isolated atoms, IE (eV) interlayer energy, evaluated as the difference between the bulk energy and the energy of an isolated two-dimensional layer, after correction for the BSSE.

	HF	B3LYP	PP	LV
Ba	−24.874 01	−25.168 26	−25.209 53	−25.123 94
F	−99.374 01	−99.700 65	−99.701 67	−99.070 88
Cl	−459.449 14	−460.038 29	−460.106 26	−458.629 60
BaFCl	−584.133 83	−585.453 42	−585.549 87	−583.418 02
BaFCl (Slab)	−584.124 49	−585.443 66	−585.537 97	−583.401 31
ΔE_f (BaFCl)	11.882	14.863	14.487	16.152
IE	0.254	0.266	0.324	0.455

The elastic constants are reported in table 4, together with the experimental data [6]. Since LV describes BaFCl as more compact and rigid than it really is (this is the usual feature for this functional), the quality of the LV results is in general lower than that obtained with PP and B3LYP. With a few exceptions (C_{33}, C_{66} and C_{12} at PP level; C_{44} and C_{12} at B3LYP level; and C_{33} and C_{12} at HF level, which differ from experiment, in absolute value, by 10.0, 26.5, 36.2, 9.7, 17.0, 12.9 and 30.9%, respectively) all the components of the elastic tensor at HF, PP and B3LYP deviate from experiment by less than 8%.

Table 3. Mulliken net atomic charges (q) and bond populations for BaFCl computed with different Hamiltonians. Data in $|e|$.

	HF	B3LYP	PP	LV
q(Ba)	+1.925	+1.875	+1.849	+1.858
q(F)	−0.949	−0.931	−0.915	−0.921
q(Cl)	−0.976	−0.944	−0.935	−0.937
b(Ba–F)	−0.025	−0.021	−0.021	−0.025
b(Ba–Cl)	−0.006	−0.003	−0.003	−0.006
b(F–Cl)	−0.003	−0.002	−0.002	−0.007

Table 4. Elastic constants C_{ij} (GPa) of BaFCl for each Hamiltonian. Percentage deviation with respect to the experimental selected values given in [5] are enclosed in parentheses.

	HF	B3LYP	PP	LV	Exp. [5]
C_{11}	71.1 (−6.3)	72.3 (−4.7)	82.8 (+8.3)	101.8 (+25.4)	75.9 ± 0.2
C_{33}	57.2 (−12.9)	61.6 (−6.2)	73.0 (+10.0)	88.7 (+25.9)	65.7 ± 0.3
C_{44}	20.2 (−0.9)	18.4 (−9.7)	20.8 (+2.0)	27.0 (+24.5)	20.38 ± 0.03
C_{66}	25.8 (+7.8)	24.5 (+2.9)	32.4 (+26.5)	35.6 (+33.1)	23.8 ± 1.1
C_{12}	19.5 (−30.9)	23.4 (−17.0)	18.0 (−36.2)	30.7 (+8.1)	28.2 ± 1.2
C_{13}	30.7 (−3.8)	33.5 (+4.8)	31.6 (−0.9)	46.4 (+31.3)	31.9 ± 1.1

Table 5. Linear compressibilities along the directions parallel ($\chi_\parallel \times 10^3$ GPa^{-1}) and perpendicular ($\chi_\perp \times 10^3$ GPa^{-1}) to the C_4 axis, volume compressibilities ($\chi \times 10^3$ GPa^{-1}) and the corresponding bulk and linear moduli (B_0, $B_\parallel$ and $B_\perp$, in GPa). Percentage deviation with respect to experiment enclosed in parentheses.

	HF	B3LYP	PP	LV	Exp. [5]
$\chi_\parallel$	8.9 (+8.5)	7.9 (−3.7)	7.0 (−14.6)	5.3 (−35.4)	8.2
$\chi_\perp$	8.0 (+11.1)	7.7 (+6.9)	7.7 (+6.9)	5.7 (−20.8)	7.2
χ	24.9 (+10.2)	23.3 (+3.1)	22.4 (−0.9)	16.7 (−26.1)	22.6
$(\chi_\perp/\chi_\parallel)$	0.90 (+2.3)	0.97 (+10.2)	1.10 (+25.0)	1.08 (+22.7)	0.88
B_0	40.2 (−9.0)	42.9 (−2.9)	44.6 (+0.9)	59.9 (+34.6)	44.2
$B_\parallel$	112.4 (−7.9)	126.6 (+3.8)	142.9 (+17.1)	188.7 (+54.7)	122
$B_\perp$	125.0 (−10.0)	129.9 (−6.5)	129.9 (−6.5)	175.4 (+26.3)	138.9

The linear compressibilities parallel ($\chi_\parallel$) and perpendicular ($\chi_\perp$) to the C_4 axis, and the volume compressibilities (χ) as well as the bulk ($B_0 = 1/\chi$) and linear ($B_\parallel = 1/\chi_\parallel$, $B_\perp = 1/\chi_\perp$) moduli deduced from the calculated elastic constants are listed in table 5, together with the experimental data. As expected, except at the LV level, all the computed values are consistent with experiment. The LV value of the bulk modulus is very close to an earlier LDA calculation [13] of 62 GPa obtained with a TB-LMTO method.

The dielectric constant and effective dynamical charge components, used for the calculation of the LO–TO splitting, are given in table 6. The tensors are diagonal, with $e^*_{xx} = e^*_{yy} = e^*_\perp$; in all cases the $e^*_\parallel$ and $e^*_\perp$ components are very similar, so that the tensor is nearly isotropic. This is even more true for the dielectric tensor, where the differences are always smaller than 0.01. The Born charges are larger than the formal charges (+2 and $-1|e|$), indicating a relatively high polarizability of the atoms. As usual, HF and LV are at the two extremes, but the differences for the e^* tensor are less than 10%. They are, in contrast, as large as 40% for ε_∞ (from 2.08 to 2.87), with B3LYP and PP in between the two extremes, and B3LYP is closest to HF.

Table 6. Effective dynamical charges along ($e^*_\parallel$) and perpendicular ($e^*_\perp$) to the C_4-axis for each ion, and dielectric constant components, calculated with the four Hamiltonians.

		HF	B3LYP	PP	LV
Ba	$e^*_\perp$	2.471	2.590	2.623	2.656
	$e^*_\parallel$	2.454	2.570	2.610	2.629
F	$e^*_\perp$	−1.267	−1.326	−1.344	−1.379
	$e^*_\parallel$	−1.303	−1.384	−1.416	−1.472
Cl	$e^*_\perp$	−1.201	−1.264	−1.285	−1.285
	$e^*_\parallel$	−1.140	−1.182	−1.194	−1.159
	$\varepsilon_\infty(xx)$	2.084	2.417	2.628	2.867
	$\varepsilon_\infty(zz)$	2.085	2.422	2.638	2.857

Table 7. Calculated and experimental Raman and infrared active modes (in cm^{-1}). The percentage deviations with respect to experimental data, given in the last column [15], are enclosed in parentheses. Δ_R and Δ_{IR} stand for the mean percentage absolute errors with respect to experiment for the set of Raman and IR frequencies, respectively.

		HF	B3LYP	PP	LV	Exp. [57]	Exp. [15]
Raman	A_{1g}	127 (−3.8)	125 (−5.3)	129 (−2.3)	144 (+8.3)	125	132
		178 (+2.8)	160 (−7.5)	164 (−5.2)	177 (+2.3)	162	173
	B_{1g}	242 (+12.4)	208 (−1.9)	209 (−1.4)	242 (+12.4)	212	212
	E_g	91 (+6.6)	78 (−8.2)	79 (−7.1)	84 (−1.2)	89	85
		152 (+9.9)	136 (−0.7)	137 (0.0)	159 (+13.8)	142	137
		280 (+11.8)	253 (+2.4)	250 (+1.2)	279 (+11.5)	247	247
	Δ_R	7.9	4.3	2.9	8.3		
Infrared	A_{2u} (TO)	129 (−0.8)	122 (−6.2)	135 (+3.7)	162 (+19.8)		130
		307 (+7.8)	283 (0.0)	281 (−0.7)	309 (+8.4)		283
	A_{2u} (LO)	194 (+2.1)	189 (−0.5)	195 (+2.6)	209 (+9.1)		190
		353 (+4.2)	332 (−1.8)	331 (−2.1)	361 (+6.4)		338
	E_u (TO)	127 (−3.1)	110 (−16.0)	115 (−12.2)	144 (+9.0)		131
		236 (+9.3)	195 (−8.9)	204 (−4.7)	243 (+11.9)		214
	E_u (LO)	159 (−1.9)	140 (−13.6)	144 (−11.1)	169 (+4.1)		162
		313 (+6.1)	285 (−3.1)	290 (−1.4)	320 (+8.1)		294
	Δ_{IR}	4.4	6.3	4.8	9.6		

We can now consider the phonon spectra at the Γ point. Group theory analysis applied to the $P4/nmm$ group predicts a distribution of the 18 degrees of freedom (two BaFCl molecules in the unit cell) into modes belonging to the following irreducible representations [57–59]:

$$\Gamma_{18} = 2A_{1g} + B_{1g} + 3E_g + 3A_{2u} + 3E_u$$

with six Raman active modes ($2A_{1g}$, $1B_{1g}$, $3E_g$), four IR active modes ($2A_{2u}$ and $2E_u$), and two acoustic modes (A_{2u} and E_u) yielding zero frequencies as the phonon wavevector $q \mapsto 0$.

In table 7 the phonon vibrational frequencies, as well as the available experimental data [15, 57], are given. The agreement between theoretical and experimental frequencies is remarkably good for the Raman mode frequencies. The mean absolute percentage difference is 2.9 and 4.3% at PP and B3LYP level, respectively, whereas it rises to 7.9 and 8.3 for HF and LV. For IR, the errors are slightly larger (4.4, 6.3, 4.8 for HF, B3LYP and PP, rising to 9.6% for LV).

Table 8. Effect of isotopic substitution on B3LYP harmonic frequencies of bulk BaFCl. $\Delta\omega$ stands for the deviation of harmonic frequencies of the isotopically substituted bulk with respect to non-substituted system; in the NORM column, the $\Delta\omega$ column is multiplied by a normalizing factor such that the largest shift is equal to 10 cm^{-1} for each isotopic substitution. The harmonic frequency shifts in going from bulk to a single layer are also reported in the last column. All data in cm^{-1}.

		Bulk	^{136}Ba		^{37}Cl		^{22}F		Slab
Mode	Symmetry	ω	$\Delta\omega$	NORM	$\Delta\omega$	NORM	$\Delta\omega$	NORM	$\Delta\omega$
1	E_g	253	0.02	0.3	−0.04	0.1	−17.54	10.0	+2.0
1′	E_u	195	0.13	1.6	−0.04	0.1	−12.35	7.0	+3.0
2	B_{1g}	208	0.00	0.0	0.00	0.0	−14.73	8.4	−4.0
2′	A_{2u}	283	0.07	0.9	−0.73	1.8	−17.24	9.8	−51.0
3	A_{1g}	160	0.08	1.0	−4.07	10.0	0.00	0.0	+8.0
3′	A_{2u}	122	0.22	2.6	−2.41	5.9	−0.32	0.2	−22.0
4	E_g	136	0.04	0.5	−3.54	8.7	−0.10	0.1	+34.0
4′	E_u	110	0.15	1.7	−2.44	6.0	−0.03	0.0	+6.0
5	A_{1g}	125	0.86	10.0	−0.26	0.6	0.00	0.0	+37.0
6	E_g	78	0.54	6.3	−0.10	0.2	−0.06	0.0	+8.0

The modes have been analysed in terms of atomic displacements both graphically [60] and by using isotopic substitutions as a complementary tool. The mass-weighted Hessian matrix has been re-diagonalized by substituting subsequently ^{138}Ba (isotopic abundance of 72%) by ^{136}Ba (isotopic abundance of 8%); ^{35}Cl (isotopic abundance of 76%) by ^{37}Cl (isotopic abundance of 24%). ^{19}F has a 100% natural abundance; in order to identify the F contribution to the modes, we used a fictitious mass of ^{22}F. The B3LYP results are given in table 8. For clarity, the frequency shifts have also been scaled in such a way that the largest shift for each isotopic substitution is equal to 10 cm^{-1} (see the NORM column). Because of the layered structure of BaFCl, we also performed the calculation of the vibrational spectra of a single two-dimensional layer containing two atomic units, whose energy is given in table 2. The F column in table 8 shows very clearly that the four modes with the highest frequency involve essentially the F atoms, with a shift ranging from 12 to 17 cm^{-1}, whereas all the other modes shift by less than 0.5 cm^{-1}. These modes are labelled as 1, 1′ and 2, 2′ in figure 3. Modes 1 and 1′ (at 195 and 283 cm^{-1}) are in-plane vibrations, and their frequency is essentially the same in the bulk and in the slab. The E_u mode is about 60 cm^{-1} lower than the E_g mode, because in the former atoms on the same plane move in the same direction, reducing the electrostatic repulsion.

For the displacements along the C_4 axis, the B_{1g} mode at 208 cm^{-1} has lower frequency (about 70 cm^{-1}) than the A_{2u} mode, because it avoids the strong polarization of the crystal that takes place in the latter; B_{1g} is about the same in the bulk and in the slab, whereas A_{2u} increases by about 50 cm^{-1} in the slab, due to the lack of compensating effects from the other layers.

Let us now consider the modes involving mainly the Cl atoms; in table 8, the Cl column shows that a shift ranging between 2.4 and 4.1 cm^{-1} is observed for the 3, 3′, 4, 4′ modes, whereas for all the other modes the ^{37}Cl isotopic shift never exceeds 0.7 cm^{-1}. The two in-plane modes at 136 and 110 cm^{-1} (3 and 3′) parallel the behaviour of 1 and 1′, the 'u' versus 'g' split being smaller here than there (26 versus 58 cm^{-1}). In the E_g case, the difference between bulk and slab is relatively large, because the Cl ions belonging to adjacent layers move in opposite directions, generating some Cl–Cl repulsion (the frequency in the layer is

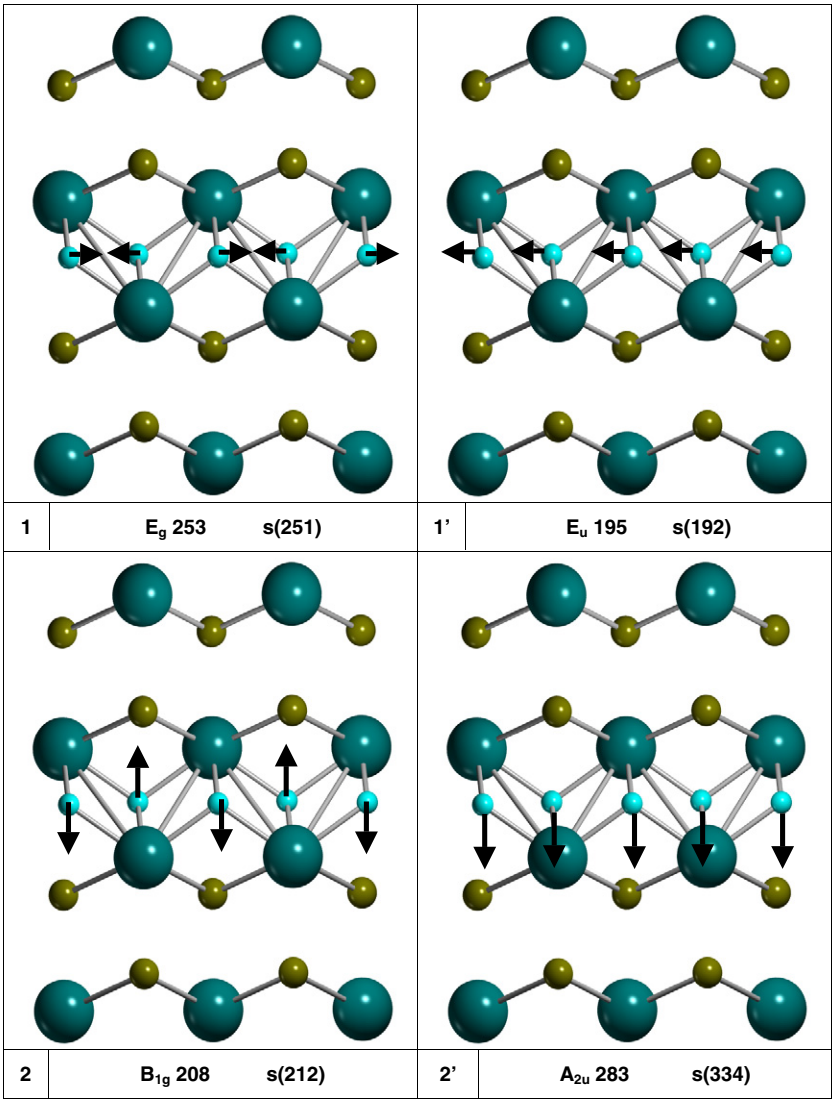

Figure 3. Atomic displacements for all normal modes and frequencies. The arrows show the motions of atoms in a complete layer and parts of the adjacent layers. Frequencies for the single two-dimensional layer are indicated as s(value). All data in cm^{-1}.

lower). This interlayer effect is much smaller in E_u (only 6 cm^{-1}) because the Cl atom of adjacent layers move in phase. Also the splitting between the A_{1g} and A_{2u} (4 and 4′) is smaller than for 2 and 2′ (38 versus 75 cm^{-1}); due to the position of the Cl atoms in the slab, the ungerade frequency is lower than the gerade one. The interlayer interaction is higher than for the F modes: it is about 8 cm^{-1} in A_{1g} (the slab frequency is lower) and 21 cm^{-1} in A_{2u}, where it increases in going from bulk to slab due to the lack of attraction from the Ba on the Cl atoms of the adjacent layers.

The last two modes, 5 and 6, at very low frequency, mainly involve the Ba atom (see table 8, where a shift of 0.86 and 0.54 cm^{-1} is observed for these two modes, whereas the

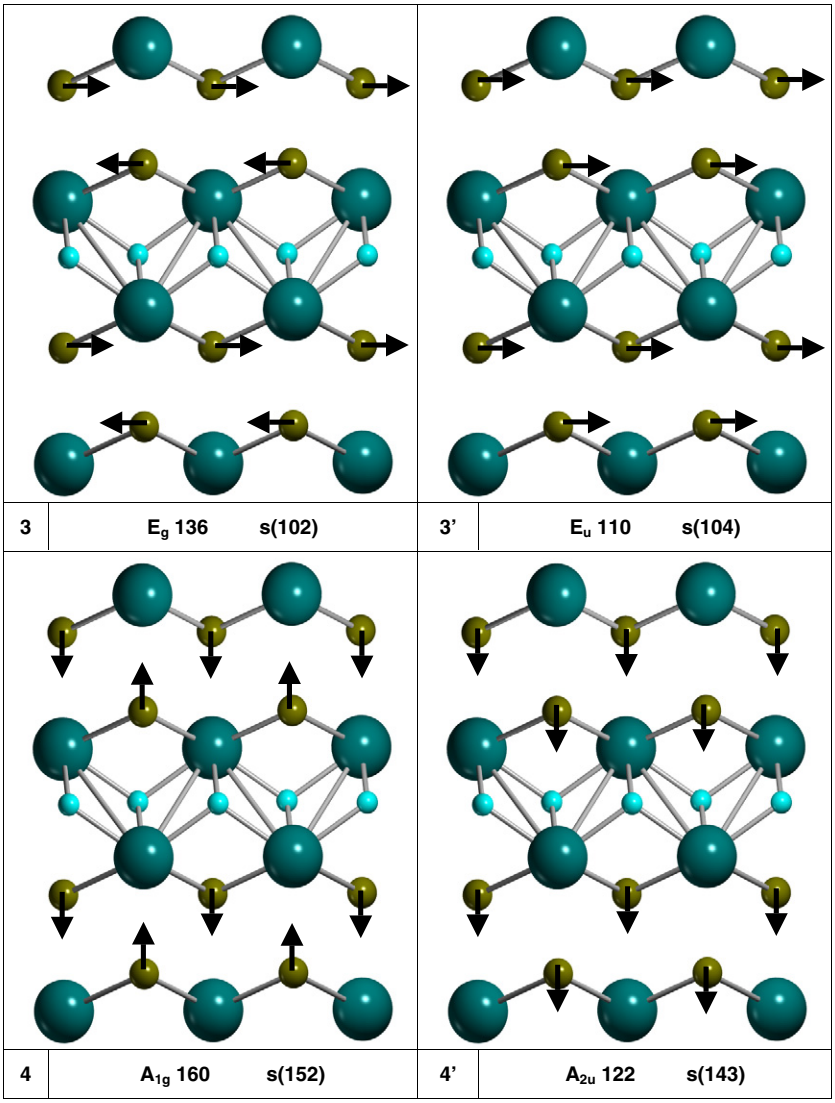

Figure 3. (Continued.)

highest ^{136}Ba shift for all the other modes is just 0.22 cm^{-1}). The isotopic effect for Ba is quite small because the masses of the two isotopes differ by 1.5% only, whereas in the Cl and F cases, they differ by 6% and 14%, respectively. These two modes, represented in the last part of figure 3, are essentially the relative motion of the two BaFCl units, in the (x, y) plane and in the z direction.

Mittal *et al* [18] recently reported similar calculations on alkaline-earth fluorohalides by using a shell model with transferable interatomic potentials. Their results on BaFCl are in good agreement with experiment. Overall, the average absolute deviation with respect to experiment for the lattice parameters, elastic constants, bulk modulus, IR and Raman frequencies are within 1%, 14%, 4%, 6% and 7%, respectively, and close to the present B3LYP results. Shell model calculations are a cheaper alternative to *ab initio* methods, but they are based on a specific

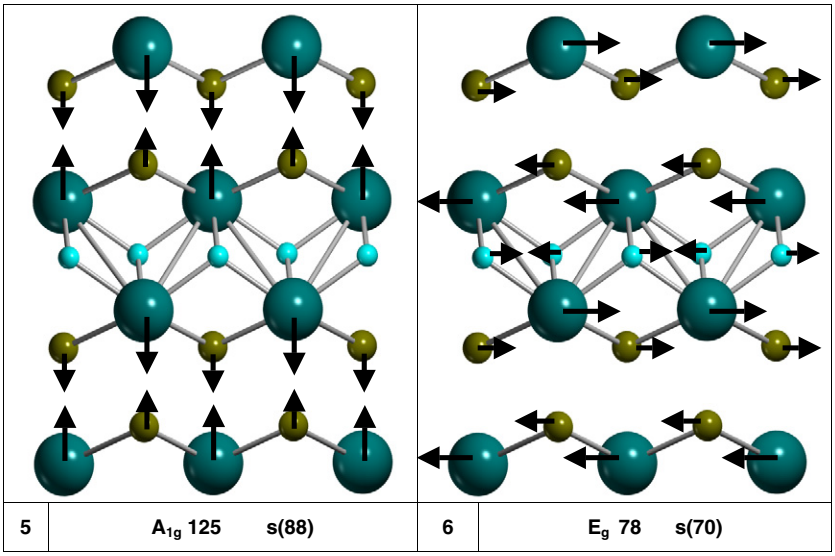

Figure 3. (Continued.)

parametrization of the model potential making them less transferable to other systems. This limits their applicability, then, to other systems, such as doped alkaline-earth fluorohalides, for which further parameters should be available.

4. Conclusion

The electronic, structural, elastic and vibrational properties of BaFCl have been computed at the *ab initio* level with four different Hamiltonians. A full analysis and classification of the vibrational modes has been performed. Good agreement with experiment has been obtained with B3LYP and PP (the former performing slightly better than the latter), whereas HF and LV provide in many cases results of lower quality. A similar performance for B3LYP was also observed for other materials [52–54]. The poor performance of HF and LV suggests that correlation effects are very important and must be properly taken into account for an accurate description of systems like BaFCl where polarization and charge transfer effects play a crucial role. New exchange–correlation functionals [61, 62] have recently been proposed that are claimed to provide a better description of such effects. Unfortunately, they are not yet implemented in the periodic *ab initio* code here adopted. Present results show the feasibility and accuracy of *ab initio* studies for heavy alkali-earth fluorohalides. They also represent a good starting point for future work on doped systems.

Acknowledgments

This work was supported in part by 'Centre National de la Recherche Scientifique' (CNRS) and the 'Ministère de l'Enseignement Supérieur et de la Recherche' (MESR). Some of the calculations were carried out on the IBM/SP3 computer at the 'Centre Informatique National de l 'Enseignement Supérieur' (CINES). We thank the scientific council of IDRIS for its support to this project.

References

[1] Sundarakannan B, Ravindran T R, Kesavamoorthy R and Satyanarayana S V M 2002 *Solid. State Commun.* **124** 385
[2] Liu M, Kurobori T and Hirose Y 2001 *Phys. Status Solidi* b **225** 20
[3] Subramanian N, Chandra Shekar N V, Sahu P Ch, Yousuf M and Govinda Rajan K 1998 *Phys. Rev.* B **58** 555
[4] Pasero M and Perchiazzi N 1996 *Mineral. Mag.* **60** 833
[5] Fischer M, Sieskind M, Polian A and Lahmar A 1993 *J. Phys.: Condens. Matter* **5** 2749
[6] Fischer M, Polian A and Sieskind M 1994 *J. Phys.: Condens. Matter* **6** 10407
[7] Beck H P, Limmer A, Denner W and Schulz H 1983 *Acta Crystallogr.* **39** 401
[8] Brixner L H, Bierlein J D and Jhonson V 1980 Eu^{2+} fluorescence and its application in medical x-ray intensifying screens *Current Topics in Material Science* vol 4, ed E Kaldis (Amsterdam: North-Holland)
[9] Blasse G 1993 *Solid State Luminescence-Theory Materials and Devices* ed A H Kitai (London: Chapman and Hall) chapter 11, p 349 and references therein
[10] Lakhshmanan A R and Govinda Rajan K 1994 *Radiat. Prot. Dosim.* **55** 247
[11] Kurobori T, Kozake S, Kawamoto T and Hirose Y 2000 *Japan. J. Appl. Phys.* **39** 537
[12] Kurobori T, Liu M, Tsunekawa H, Hirose Y and Takeuchi M 2002 *Radiat. Eff. Defects Solids* **157** 799
[13] Kalpana G, Palanivel B and Shameem Banu I B 1997 *Phys. Rev.* B **56** 3532
[14] Kalpana G, Palanivel B, Venkatasubramaniam K and Rajagopalan M 1997 *Bull. Mater. Sci.* **20** 461
[15] Sieskind M, Ayadi M and Zachmann G 1986 *Phys. Status Solidi* **136** 489
[16] Balasubramanian K R and Haridasan T M 1981 *J. Phys. Chem. Solids* **42** 667
[17] Balasubramanian K R, Haridasan T M and Krishnamurthy N 1979 *Chem. Phys. Lett.* **67** 530
[18] Mittal R, Chaplot S L, Sen A, Achary S N and Tyagi A K 2002 *Appl. Phys.* A **74** 1109
[19] Decremps F, Fischer M, Polian A and Itié J P 1998 *Eur. Phys. J.* B **5** 7
[20] Decremps F, Fischer M, Polian A and Itié J P 1999 *Phys. Rev.* B **59** 4011
[21] Shen Y R, Gregorian T and Holzapel W B 1991 *High Pressure Res.* **7** 73
[22] Shen Y R, Englisch U, Chudinovskikh L, Porsch F, Haberkorn R, Beck H P and Holzapfel W B 1993 *J. Phys.: Condens. Matter* **6** 3197
[23] Sonada M, Takano M, Miyahara J and Kato H 1991 *Radiology* **148** 833
[24] Takahashi K, Miyahara J and Shibahara Y 1985 *J. Electrochem. Soc.* **132** 1492
[25] Wyckoff R W 1948 *Crystal Structure* (New York: Interscience)
[26] Mittal R, Chaplot S L, Sen A, Achary S N and Tyagi A K 2003 *Phys. Rev.* B **67** 134303
[27] Saunders V R, Dovesi R, Roetti C, Orlando R, Zicovich-Wilson C M, Harrison N M, Doll K, Civalleri B, Bush I J, D'Arco P and Llunell M 2003 *CRYSTAL03 User's Manual (Università di Torino, Torino)*
[28] Dirac P A M 1939 *Proc. Camb. Phil. Soc.* **26** 376
[29] Perdew J P and Wang Y 1986 *Phys. Rev.* B **33** 8800
[30] Perdew J P and Wang Y 1989 *Phys. Rev.* B **40** 3399
[31] Perdew J P and Wang Y 1992 *Phys. Rev.* B **45** 13244
[32] Perdew J P 1991 *Electronic Structure of Solids* (Berlin: Akademie)
[33] Becke A D 1993 *J. Chem. Phys.* **98** 5648
[34] Lee C, Yang W and Parr R G 1988 *Phys. Rev.* B **37** 785
[35] Harrison N M and Saunders V R 1992 *J. Phys.: Condens. Matter* **4** 3873
[36] Catti M, Dovesi R, Pavese A and Saunders V R 1991 *J. Phys.: Condens. Matter* **3** 4151
[37] Hay P J and Wadt W R 1985 *J. Chem. Phys.* **82** 270
[38] Hay P J and Wadt W R 1985 *J. Chem. Phys.* **82** 284
[39] Hay P J and Wadt W R 1985 *J. Chem. Phys.* **82** 299
[40] *LoptCG (Shell Procedure for Numerical Gradient Optimisations)* written and developed by Zicovich-Wilson C M 1998 Universidad Autonoma del Estado de Morelos, Mexico
[41] Doll K, Harrison N M and Saunders V R 2001 *Int. J. Quantum Chem.* **82** 1
[42] Doll K 2001 *Comput. Phys. Commun.* **137** 74
[43] Orlando R, Saunders V R and Dovesi R 2002 unpublished
[44] Schlegel H B 1982 *J. Comput. Chem.* **3** 214
[45] Civalleri B, D'Arco Ph, Orlando R, Saunders V R and Dovesi R 2001 *Chem. Phys. Lett.* **348** 131
[46] Vosko S H, Wilk L and Nusair M 1980 *Can. J. Phys.* **58** 1200
[47] Pascale F, Zicovich-Wilson C M, Lopez Gejo F, Civalleri B, Orlando R and Dovesi R 2004 *J. Comput. Chem.* **25** 888
[48] Born M and Huang K 1954 *Dynamical Theory of Crystal Lattices* (Oxford: Oxford University Press)
[49] Umari P, Pasquarello A and Corso A D 2001 *Phys. Rev.* B **63** 094305

[50] Böttger H 1983 *Principles of the Theory of Lattice Dynamics* (Weinheim: Physick-Verlag)
[51] Liebich B and Nicollin D 1977 *Acta Crystallogr.* B **33** 2790
[52] Mérawa M, Llunell M, Orlando R, Gelize-Duvignau M and Dovesi R 2003 *Chem. Phys. Lett.* **368** 7
[53] Mérawa M, Labéguerie P, Ugliengo P, Doll K and Dovesi R 2004 *Chem. Phys. Lett.* **387** 453
[54] Mérawa M, Civalleri B, Ugliengo P, Noel Y and Lichanot A 2003 *J. Chem. Phys.* **119** 1045
[55] Baranek P, Lichanot A, Orlando R and Dovesi R 2001 *Chem. Phys. Lett.* **340** 362
[56] Bader R F W and Matta C F 2004 *J. Phys. Chem.* A **108** 8385
[57] Scott J F 1968 *J. Chem. Phys.* **49** 2766
[58] Bhatt H L, Srinivasan M R, Girisho S R, Rama Rao A H and Narayanan P S 1977 *Indian J. Pure Appl. Phys.* **15** 74
[59] Nicollin D and Bill H 1978 *J. Phys. C: Solid State Phys.* **11** 4803
[60] Ugliengo P 2003 http://www.theochem.unito.it/moldraw/moldraw.html MOLDRAW
[61] Xu X and Goddard W A III 2004 *Proc. Natl Acad. Sci.* **101** 2673
[62] Yanai T, Tew D P and Handy N C 2004 *Chem. Phys. Lett.* **393** 51